ORIGINAL RESEARCH

Antibacterial activity and cytocompatibility of an implant coating consisting of TiO₂ nanotubes combined with a GL13K antimicrobial peptide

Tao Li[1,2]
Na Wang[1]
Su Chen[1]
Ran Lu[1]
Hongyi Li[2]
Zhenting Zhang[1]

[1]Department of Prosthodontics, School of Stomatology, Capital Medical University, [2]Key Laboratory of Advanced Functional Materials, School of Materials and Engineering, Beijing University of Technology. Beijing, People's Republic of China

Correspondence: Zhenting Zhang
Department of Prosthodontics, School of Stomatology, Capital Medical University, Tian Tan Xi Li No 4, Beijing 100050, People's Republic of China
Tel +86 10 5709 9007
Fax +86 10 5709 9279
Email zztttxl@hotmail.com

Hongyi Li
Key Laboratory of Advanced Functional Materials, School of Materials and Engineering, Beijing University of Technology, Ping Le Yuan No. 100, Beijing 100124, People's Republic of China
Tel +86 10 6739 1101
Fax +86 10 6739 1101
Email lhy06@bjut.edu.cn

Abstract: Prevention of implant-associated infections at an early stage of surgery is highly desirable for the long-term efficacy of implants in dentistry and orthopedics. Infection prophylaxis using conventional antibiotics is becoming less effective due to the development of bacteria resistant to multiple antibiotics. An ideal strategy to conquer bacterial infections is the local delivery of antibacterial agents. Therefore, antimicrobial peptide (AMP) eluting coatings on implant surfaces is a promising alternative. In this study, the feasibility of utilizing TiO₂ nanotubes (TNTs), processed using anodization, as carriers to deliver a candidate AMP on titanium surfaces for the prevention of implant-associated infections is assessed. The broad-spectrum GL13K (GKIIKLKASLKLL-CONH2) AMP derived from human parotid secretory protein was selected and immobilized to TNTs using a simple soaking technique. Field emission scanning electron microscope, X-ray diffraction, Fourier transform infrared spectroscopy, and liquid chromatography–mass spectrometry analyses confirmed the successful immobilization of GL13K to anatase TNTs. The drug-loaded coatings demonstrated a sustained and slow drug release profile in vitro and eradicated the growth of *Fusobacterium nucleatum* and *Porphyromonas gingivalis* within 5 days of culture, as assessed by disk-diffusion assay. The GL13K-immobilized TNT (GL13K-TNT) coating demonstrated greater biocompatibility, compared with a coating produced by incubating TNTs with equimolar concentrations of metronidazole. GL13K-TNTs produced no observable cytotoxicity to preosteoblastic cells (MC3T3-E1). The coating may also have an immune regulatory effect, in support of rapid osseointegration around implants. Therefore, the combination of TNTs and AMP GL13K may achieve simultaneous antimicrobial and osteoconductive activities.

Keywords: orthopedic infections, titanium, nanotubes, antimicrobial peptide

Introduction

Titanium is widely used in dental implants because of its superior mechanical, physicochemical, and biochemical properties. However, implant-associated infections are a threat to patients. Meta-analyses show the mean prevalence rates of peri-implant mucositis and peri-implantitis are ~43% and 22%, respectively.[1] Interactions between bacteria, implant devices, and the host are complex and are important in implant-associated infections.[2] The major pathogens associated with peri-implant inflammation and bone loss are Gram-negative anaerobes, including *Prevotella* spp., *Porphyromonas* spp., and *Fusobacterium* spp.[3,4] Pathogens can be acquired shortly after the installation of implants. Moreover, as the bacterial colony grows, a protective exocellular polysaccharide matrix layer can be formed, which underlies the formation of bacterial biofilms on the implant surface. The complex biofilm formation on implant surfaces leads to

a 1,000-fold increase in antibiotic resistance compared with planktonic bacteria,[5] and the resulting infections are difficult to eliminate, which may impair proper osseointegration and lead to eventual implant failure.[6] Systemic or locally administered antibacterial therapies aimed at preventing initial bacterial infection have been proposed.[7,8] Systemic administration of antibacterial agents has many drawbacks including side effects and relatively low concentrations at the implant site, while local delivery of antimicrobial agents may provide optimal doses of antibacterial agents before biofilm formation is thought to be more effective.[9] The ideal coating for local release should provide a high release rate in the initial stage after implantation to inhibit bacterial adhesion or rapidly kill bacteria attached to the implant surfaces when the host immune system is weakened, and a subsequent continuous "prophylactic" slow release is also required.[10]

Various antibiotics have been integrated into localized drug carriers. Although these antibiotic-loaded coatings show benefits in terms of infection prophylaxis, two challenges still remain. Antibiotics released at suboptimal concentrations are likely to promote bacterial resistance, whereas high doses of antibiotics may generate cell toxicity and impair osseointegration.[11] Owing to their broad spectrum of bactericidal activity and low risk of promoting bacterial resistance, cationic antimicrobial peptides (AMPs) have been actively studied in the past decades.[12] It has been shown that a variety of AMPs present broad antimicrobial activity against both Gram-positive and Gram-negative bacteria, without inducing the development of resistant bacteria.[13] Therefore, AMPs present intriguing candidates as alternatives to conventional antibiotics.

The GL13K (GKIIKLKASLKLL-CONH2) AMP is a modified peptide (13 amino acids) based on the peptide sequence of human parotid secretory protein.[14] GL13K exhibits bactericidal activity against *Pseudomonas aeruginosa* and *Escherichia coli* and even binds with bacterial endotoxins to block their action.[15] Implant surfaces modified using GL13K present favorable physicochemical properties and have been proven to be cytocompatible with osteoblasts and human gingival fibroblasts.[16] Importantly, immunomodulatory activities of AMPs have also been reported.[17] All these data make GL13K a promising candidate for infection prevention with dental implants.

A variety of localized antimicrobial materials including calcium phosphate coatings, TiO_2 nanotubes (TNTs), and polymeric coatings have been created to counter implant-associated infections.[12,18,19] Recently, TNTs have drawn much attention in this regard. TNTs fabricated by anodizing have been reported as favorable platforms for adhesion and growth of osteoblasts, and are also beneficial for the differentiation of stem cells by mimicking the nanostructures of hydroxyapatite dispersed within bone tissue.[20,21] They can also acquire antibacterial properties by acting as carriers for bactericides.

Conventional antibiotics such as gentamicin have been doped into TNTs for prevention of bacterial infections.[22] However, reports on TNTs as carriers to deliver GL13K AMP for dental implants have been limited.

This study aims to develop antimicrobial coatings for dentistry applications by combining TNTs and GL13K using a simple soaking technique, to develop antimicrobial coatings for dentistry applications. Metronidazole (MNA) is used as a positive control. As a first step, the antimicrobial activity against bacterium putative of peri-implantitis including *Fusobacterium nucleatum* and *Porphyromonas gingivalis*, and cytocompatibility with a preosteoblastic cell line (MC3T3-E1) and mouse macrophage cell line (J774A.1) of GL13K-immobilized TNTs (GL13K-TNTs), MNA-immobilized TNTs (MNA-TNTs), and unmodified TNTs were investigated, to estimate the feasibility of using TNTs as a carrier of antibacterial agents for prevention of implant-associated infections.

Materials and methods
Fabrication of TNTs
TNTs were fabricated by anodization. The process is described as follows. Commercially pure Ti plates (Ti >99.7%; Baoji Titanium Industry Co., Ltd., Baoji, People's Republic of China) of 10×10 mm dimensions were ultrasonically and consecutively rinsed in acetone, ethanol, and distilled water for 10 min. Then, the anodization process was performed in 0.5% hydrofluoric acid solution at the voltage of 25 V for 3 h at room temperature to acquire TNTs with a diameter of 80 nm, in which Ti plates were used as the anode and graphite foil as the cathode. After anodizing, the samples were annealed at 450°C for 3 h to crystallize the amorphous TNTs to an anatase structure and then rinsed with distilled water and air dried. TNTs were sterilized by autoclaving and ultraviolet irradiation for 2 h prior to further use.

Immobilization of antibacterial agents
To immobilize the GL13K AMP (DgPeptides Co., Ltd., Hangzhou, People's Republic of China) and conventional MNA antibiotic (SOLARBIO Technology Co., Ltd., Beijing, People's Republic of China) to TNTs, 10 mg mL^{-1} of GL13K or MNA was prepared in distilled water. TNTs were immersed into either MNA solution or GL13K solution for 15 min in an ultrasound bath, and were then allowed to dry in air for 15 min at room temperature. Once dried, the loading steps mentioned above were repeated twice. After that, the

samples were gently rinsed with 1 mL of distilled water to remove any excess drug.

Surface characterization

The surface morphology of the TNTs with or without loaded antibacterial agents was assessed using a field emission scanning electron microscope (FESEM, S4800; Hitachi Ltd., Tokyo, Japan) after sputter coating with a thin layer of gold. Phase composition of TNTs before and after heat treatment was evaluated using X-ray diffraction (D8 advance; Bruker AXS, Karlsruhe, Germany) with a diffractometer with Cu Kα radiation. The chemical composition of the coatings was determined using Fourier transform infrared spectroscopy (FTIR, Spectrum 400; PerkinElmer Inc., Waltham, MA, USA) in the range of 4,000–650 cm^{-1}, while MNA and GL13K standards were used for calibration.

Release profile of antibacterial agents

In vitro release profiles of MNA and GL13K from TNTs were evaluated using liquid chromatography–mass spectrometry (LC–MS, 1,290–6,490; Agilent Technologies, Santa Clara, CA, USA). Each specimen was incubated in 1 mL of distilled water (to function as a release solution) at room temperature in a capped vial. Release solution was removed (200 µL) and replaced with 200 µL of distilled water at regular intervals (5, 10, 20, and 30 min; 1 and 2 h; 1, 2, 3, 5, and 7 days). Standard curves with known concentrations of the antibacterial agents were used as calibration curves by which drug concentrations in the release solution could be calculated. A 100×3 mm StableBond-Aq reversed-phase column packed with 1.8 µm core–shell particles was used at 25°C for liquid chromatography. An elution chromatography program for GL13K consisted of two components, 15 wt.% methanoic acid and 85 wt.% acetonitrile, while the mobile phase for MNA was 45 wt.% methanoic acid and 55 wt.% methanol. The flow rate was 0.3 mL min^{-1} and the injection volume was 2 µL.

The mass spectrometry conditions that provided optimal sensitivity were: needle voltage at 3,000 V, drying gas at 200°C and 30 psi, and the flow rate was 14 L min^{-1}. GL13K (m/z 712.4 → m/z 703.9) with collision energy of 24 eV and MNA (m/z 445.1 → 410.0) with collision energy of 14 eV were monitored through multiple ion channels.

Antimicrobial activity assessment

The antimicrobial activities of the specimens against two Gram-negative anaerobic bacterial strains, *F. nucleatum* (American Type Culture Collection [ATCC] 25586) and *P. gingivalis* (ATCC 33277), were assessed using a disk-diffusion assay (Kirby–Bauer). Both bacterial strains were characteristic of those involved in peri-implantitis. Bacteria were cultured in sterile tubes containing 5 mL of Center for Disease Control and Prevention (CDC) anaerobic medium under anaerobic conditions (80% N$_2$, 10% CO$_2$, and 10% H$_2$) at 37°C for 48 h to obtain bacteria in the mid-logarithmic phase. Bacterial suspensions were then diluted using CDC anaerobic medium to provide a final density of ~10^6 colony forming units mL^{-1}. Diluted *F. nucleatum* or *P. gingivalis* suspension (1 mL) was seeded on the surface of a CDC anaerobic agar plate and allowed to dry for 10 min. Then, GL13K-TNTs, MNA-TNTs, and unmodified TNTs were placed on the bacteria-inoculated agars. The agar plates were then incubated for 5 days under anaerobic conditions at 37°C.

Behavior of MC3T3-E1 cells on nanostructured coatings

Cell culture and seeding

MC3T3-E1 cells, a clonal mouse preosteoblastic cell line, were obtained from the Cell Resource Center, Institute of Basic Medical Sciences, Peking Union Medical College, Beijing, People's Republic of China. Cells were cultured in an alpha minimum essential medium (Thermo Fisher Scientific, Waltham, MA, USA) supplemented with heat-inactive 10% fetal bovine serum (Thermo Fisher Scientific) and 1% penicillin/streptomycin at 37°C in a humidified 5% CO$_2$ atmosphere and passaged every fifth day. The culture medium was refreshed at 2-day intervals. Confluent cells were trypsinized and resuspended in fresh culture medium for further use.

To assess the influence of specimens on cells in culture, 2×10^4 dispersed cells were seeded per well in triplicate onto the GL13K-TNTs, MNA-TNTs, and TNTs in 24-well culture plates for cell adhesion assays, proliferation assays, and morphology observations, while 3×10^4 cells per well were seeded for osteogenic differentiation assays. To induce osteogenesis, subconfluent cells were cultured in osteogenic inductive medium consisting of the above culture medium, 10^{-8} M dexamethasone (Sigma-Aldrich Co., St Louis, MO, USA), 50 µg mL^{-1} ascorbic acid (Thermo Fisher Scientific), and 10 mM β-glycerophosphate (MP Biomedicals, Santa Ana, CA, USA). The osteogenic inductive medium was replaced every second day.

Cell adhesion and proliferation

To study cell adhesion, MC3T3-E1 cells were allowed to attach for 4 h. Nonadherent cells were removed by rinsing with phosphate-buffered saline (PBS) solution; adherent cells were fixed in 4% paraformaldehyde and stained using 4′,6-diamidino-2-phenylindole (DAPI, D9542; Sigma-Aldrich Co.) for 10 min. Then, the cell numbers on each specimen were

counted in five random fields using Image-Pro Plus software under a fluorescence microscope (OLYMPUS DP71; Olympus Corporation, Tokyo, Japan) at 100× magnification.

Cell proliferation was assessed using a Cell Counting Kit-8 (CCK-8; Dojindo Molecular Technologies, Kamimashiki-gun, Kumamoto, Japan) assay after 1, 3, and 5 days of culture. At each time point, specimens with seeded cells were gently rinsed twice using PBS and transferred to new 24-well culture plates; then, 1 mL of culture medium and 100 µL of CCK-8 solution were added to each well and incubated for 4 h. Subsequently, 200 µL of each sample was transferred to a 96-well culture plate. Mean absorbance at 450 nm was measured using a microplate spectrophotometer (Model SpectraMax Plus 384).

Cell morphology

Cell morphology was examined after 24 and 48 h of incubation by fluorescent staining of actin and cell nuclei. After two rinses with PBS, cells on the samples were fixed using 4% formaldehyde and treated with 0.1% Triton X-100. Then, the samples were incubated with tetramethylrhodamine B isothiocyanate labeled phalloidin (P1951; Sigma-Aldrich Co.) for 1 h. Following three rinses with PBS, the cell nuclei were stained with DAPI for 10 min and finally examined using fluorescence microscopy.

Alkaline phosphatase activity

Alkaline phosphatase (ALP) activity is an important parameter of osteoblastic osteogenic functionality. Thus, it was measured after 7 and 14 days of culture. Cells on the samples were washed three times with PBS and lysed in 0.1% Triton X-100. Cell lysates were transferred to microcentrifuge tubes and centrifuged at 14,000 rpm for 15 min at 4°C. The supernatants were collected for evaluation of ALP activity and total protein content. ALP activities were measured using an Alkaline Phosphatase Assay Kit (Nanjing Jiancheng Bioengineering Institute, Nanjing, People's Republic of China) according to the instructions provided by the manufacturer, using *p*-nitrophenol as a standard. Absorbance of solutions was measured at 405 nm. The intracellular total protein content was determined using a Bradford assay, with ALP activities normalized to total protein concentration.

Macrophage response to nanostructured coatings

Cell adhesion and proliferation

The J774A.1 mouse macrophage cell line was obtained from the Cell Resource Center, Institute of Basic Medical Sciences, Peking Union Medical College. Cells were cultured in Dulbecco's Modified Eagle's Medium (DMEM; Thermo Fisher Scientific) supplemented with heat-inactive 10% fetal bovine serum and 1% penicillin/streptomycin at 37°C in a humidified 5% CO_2 atmosphere and passaged every 3 days.

Macrophages were seeded at 2×10^4 cells per well onto the MNA-TNTs, GL13K-TNTs, and TNTs in 24-well culture plates in triplicate and cultured for 4, 24, and 48 h to evaluate cell adhesion and proliferation using a CCK-8 assay. At each prescribed time point, specimens with seeded cells were gently rinsed twice with PBS and transferred to new 24-well culture plates; then, 1 mL of DMEM and 100 µL of CCK-8 solution were added to each well and incubated for 2 h. Subsequently, 200 µL of each sample was transferred to a 96-well culture plate. Mean absorbance at 450 nm was measured using a microplate reader.

Analysis of cell morphology

After 4 h of culture, macrophages on each sample (as described above) were rinsed with PBS for subsequent analysis of cell morphology. Macrophages were fixed with 3% glutaraldehyde at 4°C for 2 h, postfixed with 1% osmium tetroxide, and subsequently dehydrated with a graded series of alcohol (50%, 70%, 80%, 90%, and 100%) for 10 min. Then, the samples were dried in hexamethyldisilazane and sputter coated with a thin layer of gold/palladium for scanning electron microscopy observations (TM-1000 SEM; Hitachi Ltd.).

Statistical analyses

Data were analyzed using Statistical Package for the Social Sciences (SPSS) 20.0 software, and mean values derived from three sample sets for each assay were presented. Error bars represent standard error of the mean. Statistical comparisons were determined using one-way analysis of variance and post hoc Tukey's multiple comparison testing. The significance level is set at $P < 0.05$.

Results

Surface morphology

Figure 1A shows the FESEM images of TNTs after annealing. The high magnification inset shows that the pore diameter of the TNTs was ~80 nm, while a cross-sectional view shows that the TNTs were oriented vertically to the surface with a length of ~2 µm. FESEM micrographs of GL13K-TNTs and MNA-TNTs show that GL13K and MNA were doped onto and into the TNTs (Figure 1B and C). The X-ray diffraction patterns of the TNTs before and after heat treatment demonstrate that TNTs annealed at 450°C in the presence of oxygen
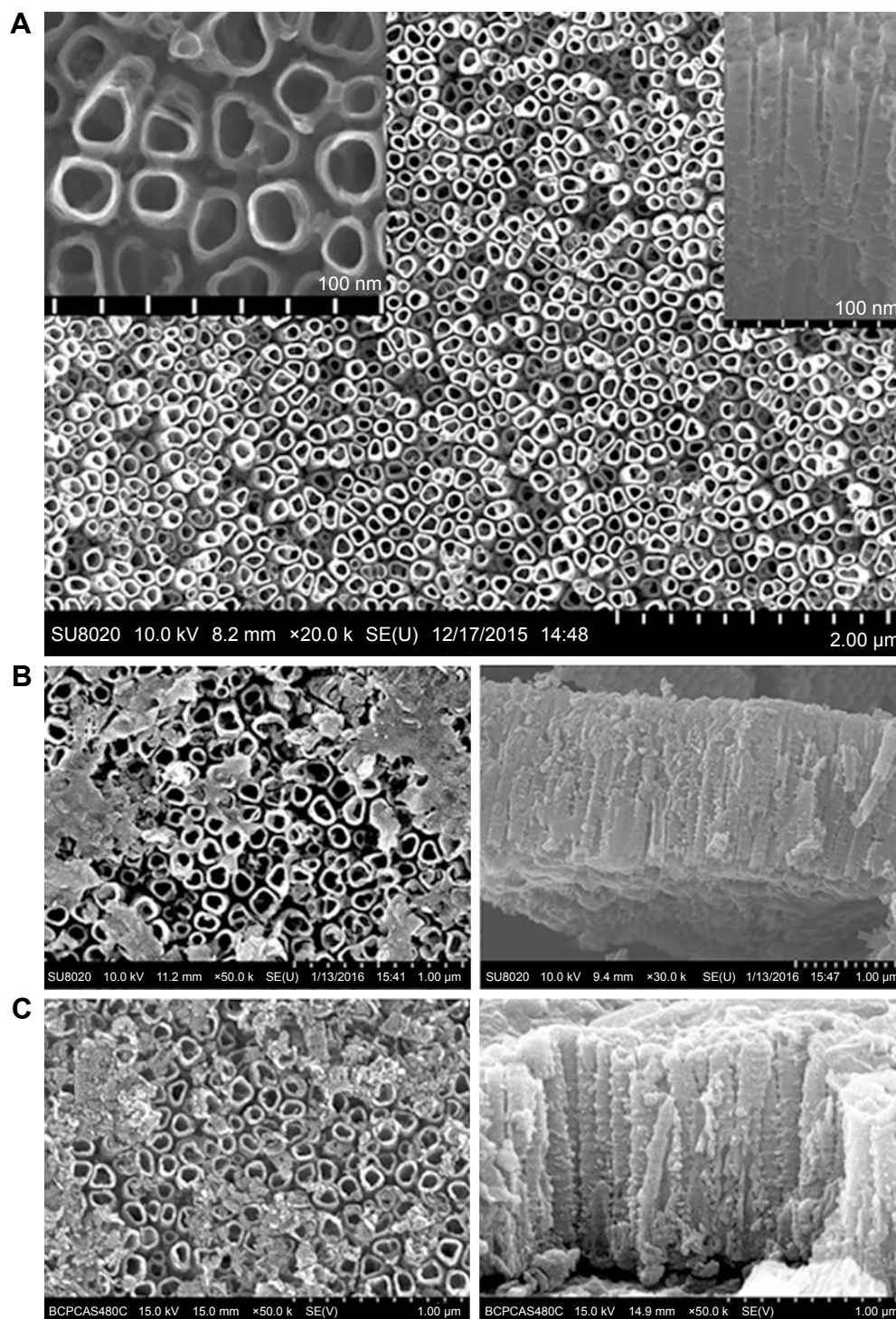
Figure 1 FESEM micrographs of TNTs after annealing (**A**) including a high-magnification inset showing the pore diameter of 80 nm and cross-sectional view showing a length of approximately 2 μm; (**B**) MNA-TNTs showing the decoration of the TNTs with MNA flakes both in top view and in cross-sectional view; (**C**) GL13K-TNTs both in top view and in cross-sectional view.
Abbreviations: FESEM, field emission scanning electron microscope; MNA, metronidazole; MNA-TNTs, MNA-immobilized TNTs; TNTs, TiO₂ nanotubes.

and in dry ambient conditions have an anatase crystalline phase (Figure 2). The FTIR spectra of TNTs, MNA-TNTs, and GL13K-TNTs are shown in Figure 3. No absorption wave was found for TNTs, as shown in Figure 3A. The absorption wave at 1,534.5 cm^{-1} is attributed to a $-NO_2$ peak in both MNA and MNA-TNT coatings (Figure 3B), while amide I and II peaks at 1,630 and 1,540 cm^{-1} (Figure 3C) indicate the presence of GL13K in the GL13K-TNTs. Moreover, the spectra of the MNA-TNT and GL13K-TNT samples are in accordance with standard MNA and GL13K spectra.
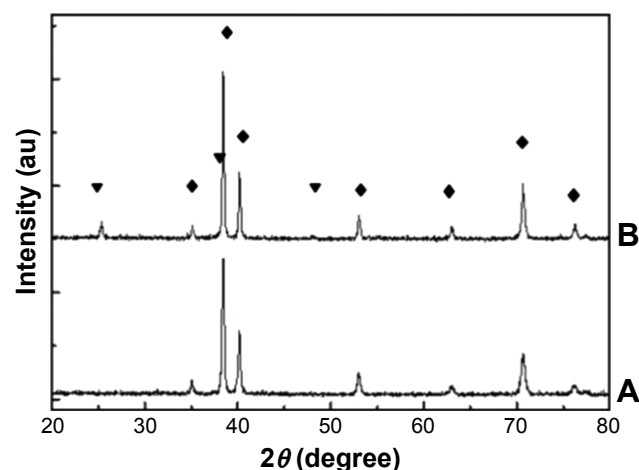
Figure 2 XRD pattern of TNTs (**A**) before and (**B**) after annealing at 450°C.
Abbreviations: TNTs, TiO$_2$ nanotubes; XRD, X-ray diffraction.

Release kinetics

Figure 4A shows the cumulative released amounts of MNA and GL13K over time after immersion of MNA-TNTs and GL13K-TNTs in distilled water. Each measurement was performed in triplicate. The cumulative amount of drug was plotted against square root of the time. As expected, a high rate of release was observed during the initial 30 min, and this was followed by a slow and sustained release. From 30 min on, the cumulative release rates of MNA and GL13K were close to the linear regression with square root of time (Figure 4B).

Antimicrobial activity

Zones of inhibition were observed as distinct clear areas around the MNA-TNT and GL13K-TNT specimens in the disk-diffusion assay (Figure 5). These results indicate that MNA- and GL13K-decorated TNTs were able to kill both *F. nucleatum* and *P. gingivalis*, but undecorated coatings did not exhibit any antimicrobial activity in the disk-diffusion assay.

Behavior of MC3T3-E1 cells on nanostructured coatings

After a 4 h incubation with MC3T3-E1 cells, the fluorescence images (Figure 6A–C) show the typical morphology of the cell nuclei on all analyzed specimens. GL13K-TNTs possessed the highest density of nuclei, which was significantly more than the other two groups. However, no significant difference in adherent cell numbers on TNTs and MNA-TNTs was observed (Figure 6D).

Cell proliferation, ALP activity, and cell morphology were also assessed to investigate the behavior of MC3T3-E1

cells on nanostructured coatings. In all cases, cells grew continuously upon interaction with the specimens for 1, 3, and 5 days. No decrease in cell numbers was detected in the GL13K-TNT group compared with the control groups. Notably, cell proliferation on the GL13K-TNT samples was significantly higher than that on the MNA-TNT samples after 1 and 5 days of culture ($P<0.05$, Figure 7A). Figure 7B shows the ALP activity normalized to total protein concentration. In comparison with the TNT and MNA-TNT groups, no significant decrease in ALP activity was detected for the GL13K-TNT group across all time points. However, for the MNA-TNT group, an obvious decrease in ALP activity was observed compared with the other two groups after 14 days of culture ($P<0.05$). The GL13K-TNT group exhibited a slightly elevated ALP activity in comparison with the TNT group, but the difference was not statistically significant. Figure 8 shows that the MC3T3-E1 cells attached closely and spread well on GL13K-TNTs and TNTs. Cells were elongated and a polygonal shape was demonstrated. However, the MNA-TNTs elicited inferior cell spreading, and most cells on this material demonstrated less microfilaments compared with those in the other two groups.

Macrophage response to nanostructured coatings

Upon culture with macrophages for 4, 24, and 48 h, statistical analysis showed that the levels of cell proliferation on GL13K-TNTs were significantly higher than those on MNA-TNTs at each prescribed time point, but were higher than those on TNTs only at 48 h ($P<0.05$, Figure 9A).

Macrophages grew and spread differently on these three surfaces, and scanning electron microscopy images revealed the evident differences in cell morphology (Figure 9B–D). On TNTs and GL13K-TNTs, the macrophages spread out with numerous cytoplasmic lamellipodia on the rim and protrusions on the surface. However, most cells on MNA-TNTs demonstrated a spindle-like shape with few lamellipodia or protrusions, and cytoplasmic perforations were observed.

Discussion

Our data demonstrated that broad-spectrum GL13K AMP can be successfully immobilized to TNTs. GL13K-decorated coatings had a strong antimicrobial effectiveness against bacterium putative of peri-implantitis, and were also biocompatible with preosteoblast and macrophage cells.

A carrier for local delivery of antibacterial agents for the prevention of implant-associated infections must possess two characteristics. First, an effective dose of antibacterial agent
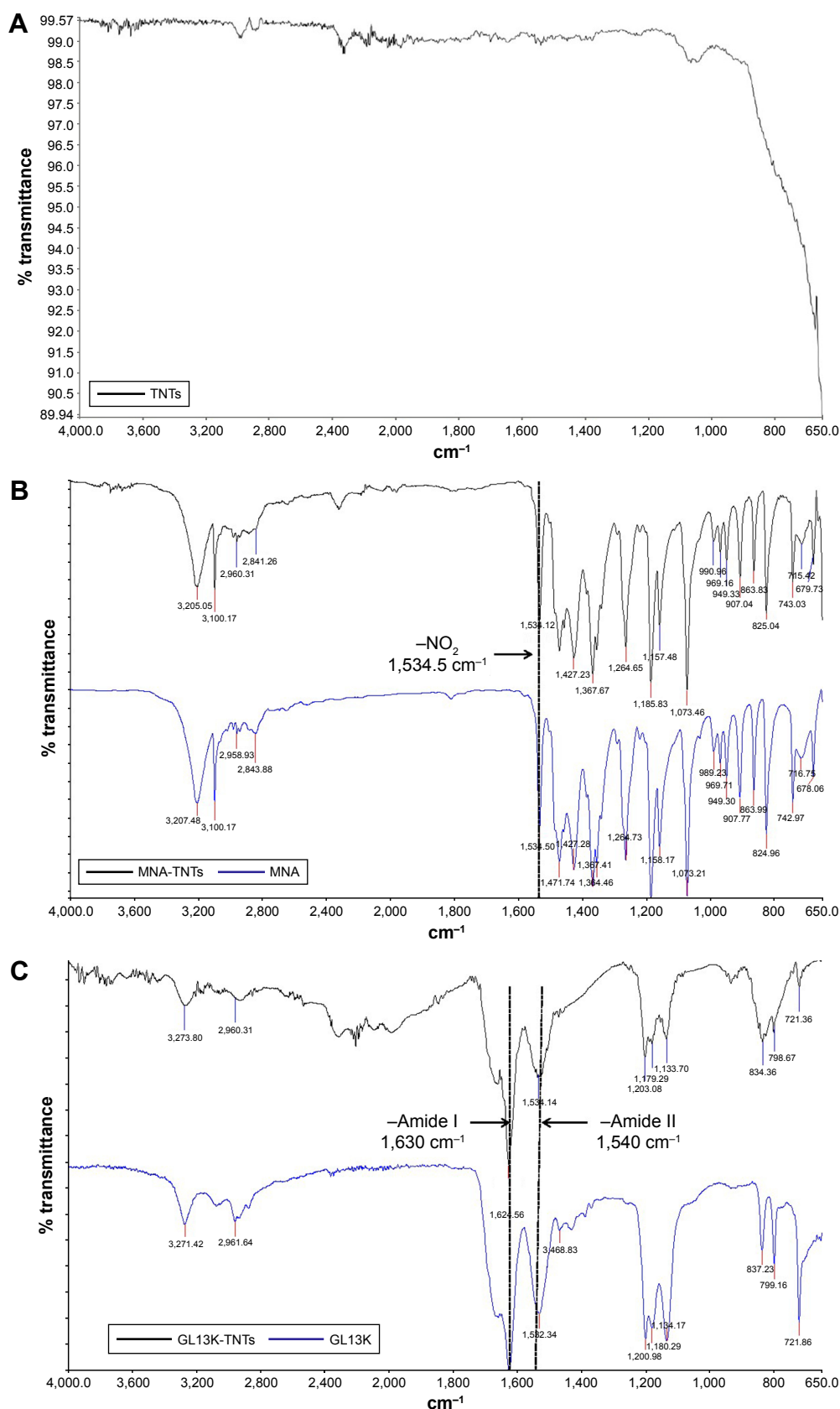
Figure 3 FTIR spectra of (**A**) TNTs with no absorption wave; (**B**) MNA-TNTs with a wave number at 1,534.5 cm^{-1} attributed to the –NO$_2$ peak from MNA; (**C**) GL13K-TNTs with amide peaks at 1,630 and 1,540 cm^{-1} from GL13K.
Abbreviations: FTIR, Fourier transform infrared spectroscopy; MNA, metronidazole; MNA-TNTs, MNA-immobilized TNTs; TNTs, TiO$_2$ nanotubes.
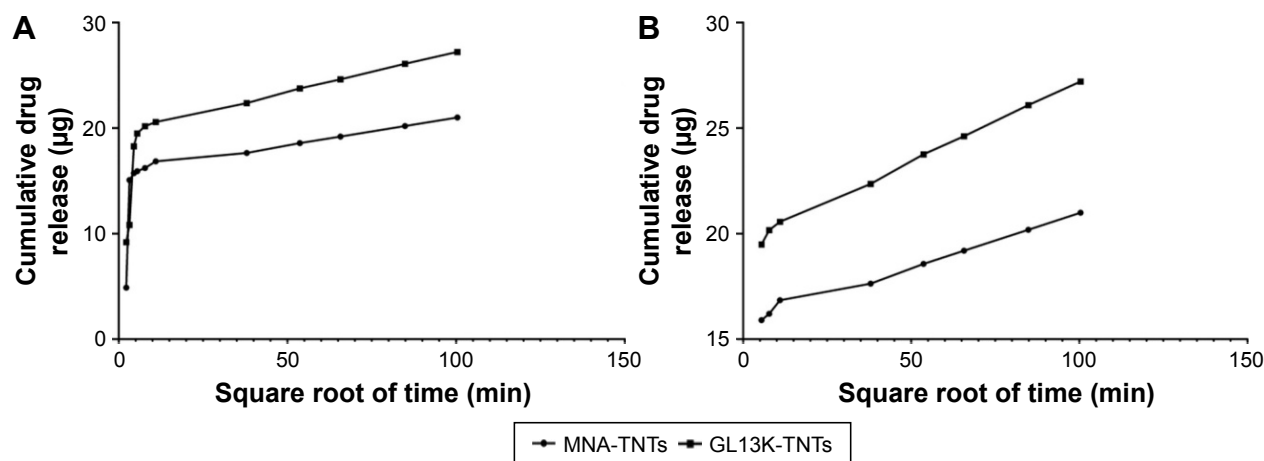
Figure 4 Release kinetics of MNA and GL13K from TNTs.
Notes: (**A**) Cumulative drug release over square root of time; (**B**) cumulative release of MNA and GL13K are close to the linear regression with square root of time from 30 min.
Abbreviations: MNA, metronidazole; TNTs, TiO_2 nanotubes.

must be placed at the implant site to provide a constant antimicrobial efficacy. Second, the carrier should not interfere with tissue remodeling and bone healing. This research group has previously demonstrated that TNTs are osteoconductive and a pore diameter of 70 nm is the optimum size,[23] and when conjugated with bone morphogenetic protein-2 knuckle peptide, such TNTs were beneficial for osteointegration.[24] ZnO nanoparticle-decorated TNTs (80 nm) have been previously developed, and have been shown to constantly release Zn ions providing antimicrobial activity and stem cell compatibility.[25] Furthermore, TNTs (80 nm) have previously been shown to promote macrophage adherence and proliferation, and suppress inflammatory cell responses.[26] Based on these findings, in this study, TNTs (80 nm) fabricated using anodization were adopted as a carrier for an antibacterial agent. All TNTs used in this study were annealed at 450°C for 3 h to crystallize

the amorphous TNTs into an anatase structure, and sterilized using ultraviolet irradiation for 2 h. Previous studies have shown that anatase TNTs are beneficial for the nucleation and growth of hydroxyapatite,[27] and when sterilized using ultraviolet irradiation, anatase TNTs can acquire photocatalytic properties accounting for improved cell behavior and early-stage bone formation.[28] In this study, TNTs were loaded with a novel GL13K AMP and a conventional MNA antibiotic. FESEM (Figure 1), FTIR (Figure 3), and LC–MS (Figure 4) analyses confirmed that GL13K and MNA were successfully immobilized onto and into 80 nm TNTs using a simple soaking technique, without any change in physicochemical properties and structure.

AMPs have potent antibacterial activity against both Gram-positive and Gram-negative bacteria. GL13K, which is designed by replacing three amino acids of $GL13NH_2$
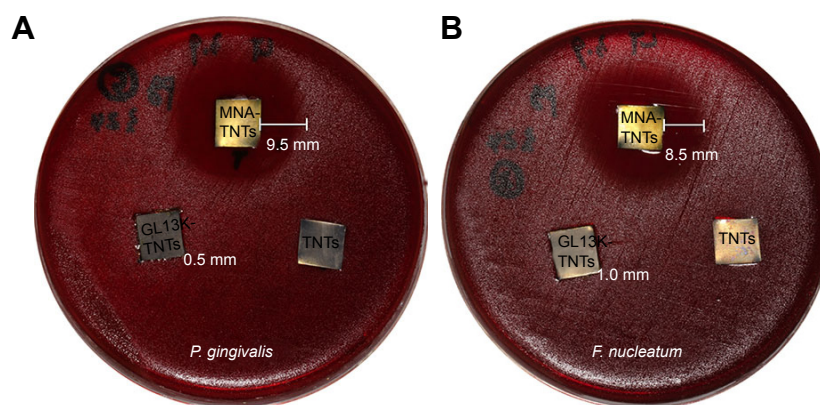

Figure 5 Evaluation of antimicrobial activity of the MNA-TNTs, GL13K-TNTs, and TNTs against (**A**) *Porphyromonas gingivalis* ATCC 33277 and (**B**) *Fusobacterium nucleatum* ATCC 25586, assessed using disk-diffusion assay.
Abbreviations: MNA, metronidazole; MNA-TNTs, MNA-immobilized TNTs; TNTs, TiO_2 nanotubes; ATCC, American Type Culture Collection.
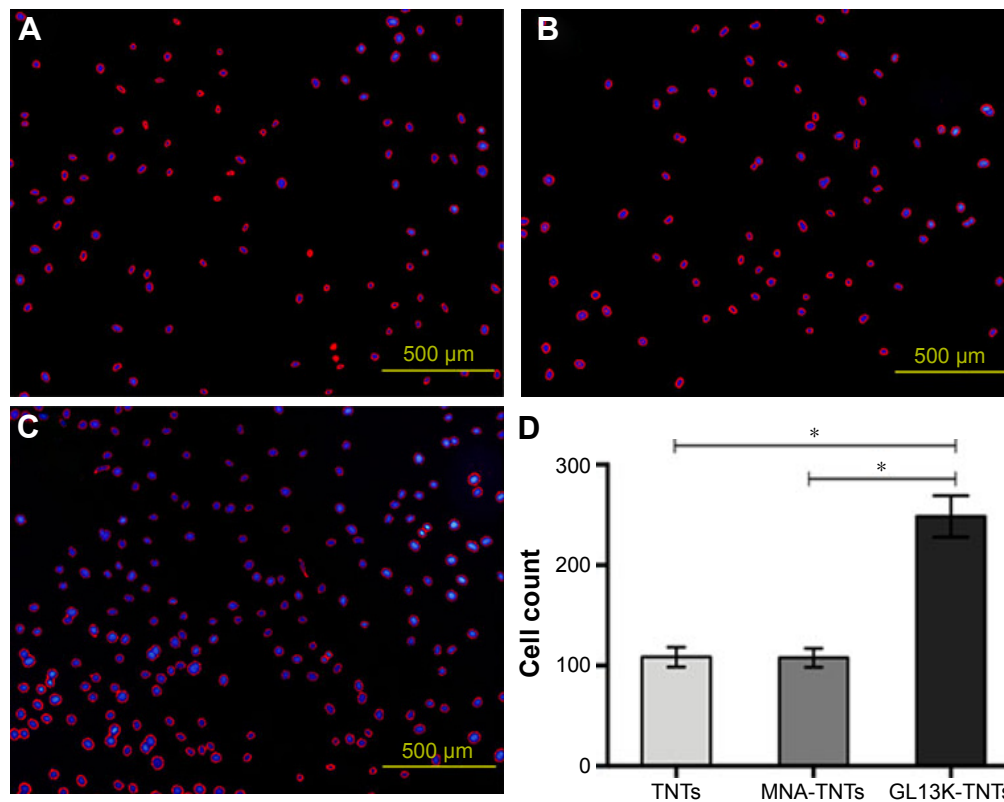
Figure 6 Fluorescence images of MC3T3-E1 cells incubated for 4 h on (**A**) TNTs, (**B**) MNA-TNTs, and (**C**) GL13K-TNTs. (**D**) Cell adhesion measured by counting the cell nuclei. *Statistical significance ($P<0.05$, n=3). Magnification: 100×.
Abbreviations: MNA, metronidazole; MNA-TNTs, MNA-immobilized TNTs; TNTs, TiO$_2$ nanotubes.

with lysine residues, has a net charge of +5 at pH 7.4. It also adopts a favorable secondary structure in accordance with its surrounding environment to develop relatively hydrophilic or hydrophobic properties.[29] The minimal inhibitory concentration of GL13K is as low as 5–10 µg mL^{-1} against *P. aeruginosa* and *E. coli*,[30] and GL13K-modified Ti surfaces

are antimicrobial against *P. gingivalis*.[16] Like other cationic AMPs, the cationic portions of GL13K interact with negatively charged bacterial membranes, and subsequently permeate or translocate across the membranes to disrupt their barrier function,[29,31] which forms the basis of their antimicrobial activities. However, GL13K does not inhibit mammalian
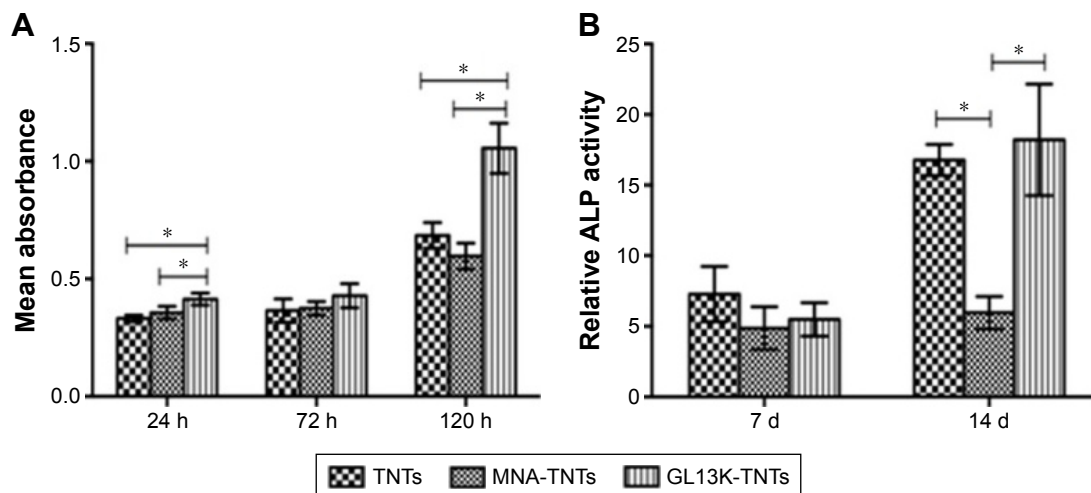

Figure 7 MC3T3-E1 cells on samples.
Notes: (**A**) Absorbance indicating the proliferation of MC3T3-E1 cells cultured on samples for 24, 72, and 120 h. (**B**) Normalized ALP activities indicating cell differentiation in samples at 7 and 14 days. *Statistical significance ($P<0.05$, n=3).
Abbreviations: ALP, alkaline phosphatase; d, days; h, hours; MNA, metronidazole; MNA-TNTs, MNA-immobilized TNTs; TNTs, TiO$_2$ nanotubes.
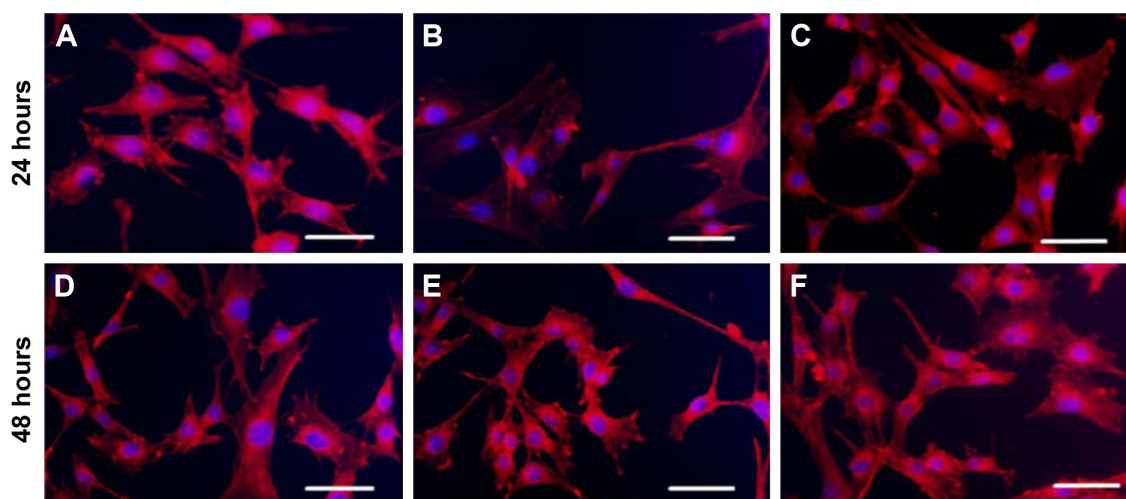
Figure 8 Fluorochrome micrography of MC3T3-E1 cells cultured for 24 and 48 h on (**A**, **D**) TNTs, (**B**, **E**) MNA-TNTs, and (**C**, **F**) GL13K-TNTs (magnification =×320; scale bar =100 μm). Actin is shown in red and cell nuclei are shown in blue. On MNA-TNTs, some cells spread poorly with less polygonal and elongated cell shapes.
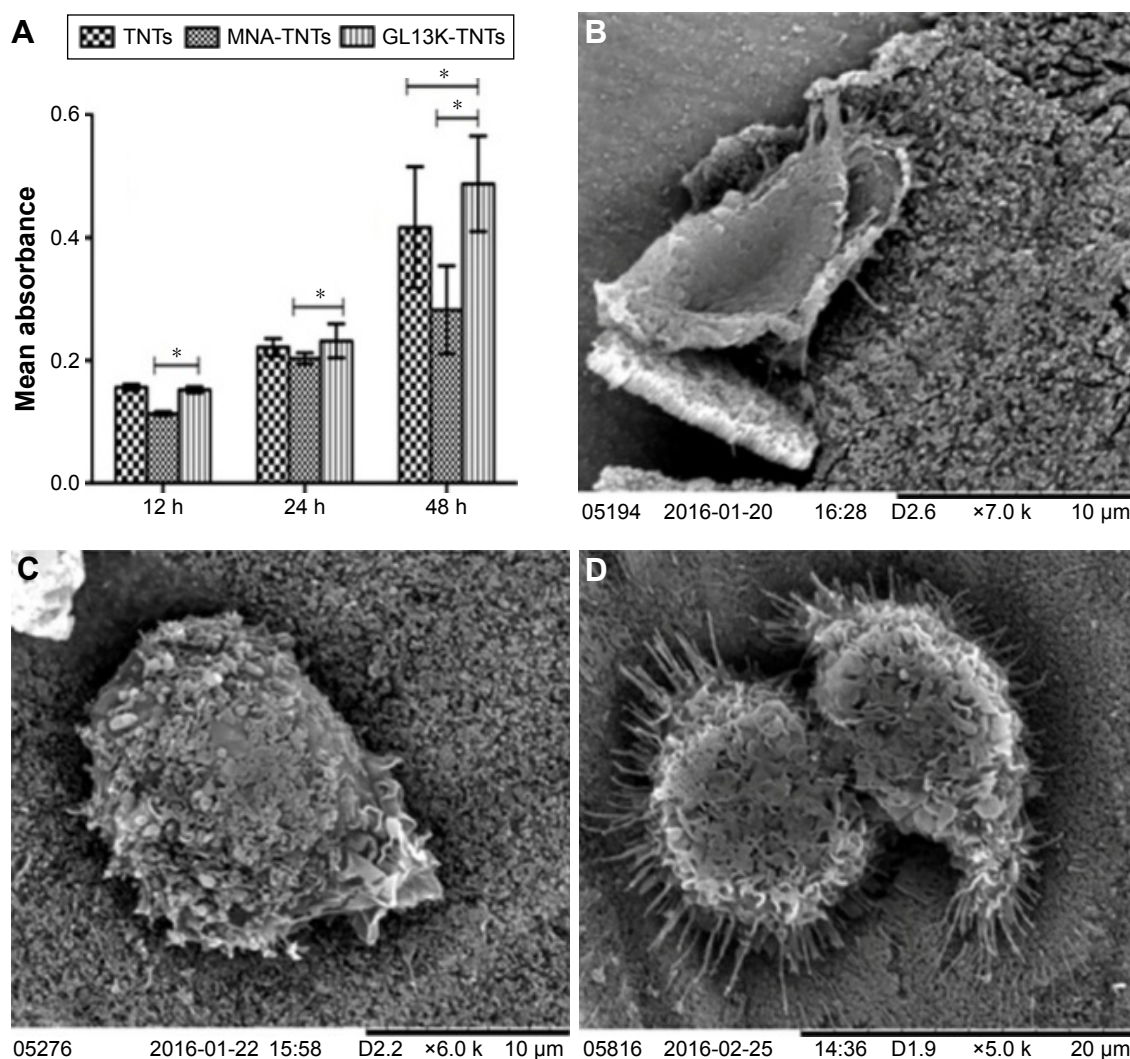**Abbreviations:** MNA, metronidazole; MNA-TNTs, MNA-immobilized TNTs; TNTs, TiO$_2$ nanotubes.

Figure 9 (**A**) CCK-8 assay used to evaluate macrophage proliferation on samples, *statistical significance ($P<0.05$, n=3). SEM images of macrophages incubated on (**B**) TNTs, (**C**) MNA-TNTs, and (**D**) GL13K-TNTs for 4 h.
Abbreviations: CCK-8, Cell Counting Kit-8; h, hours; MNA, metronidazole; MNA-TNTs, MNA-immobilized TNTs; TNTs, TiO$_2$ nanotubes.

cell proliferation or enhance macrophage inflammatory responses.[15] Therefore, GL13K may be a novel compound for use in antimicrobial and anti-inflammatory devices, with less potential to induce the formation of drug-resistant bacteria than traditional antibiotics.

LC–MS measurements in this study (Figure 4) suggest an initial burst release of MNA and GL13K in the first 30 min, which is due to the rapid diffusion of the immobilized drugs to the outermost surfaces. Subsequently, the cumulative drug release was close to the linear regression with the square root of time, suggesting a slow and stable release up to 7 days. The release profile was similar to those reported by Ma et al[32] and Lai et al,[33] who used anodized titanium as an HHC-36 or enrofloxacin hydrochloride carrier. The release profiles were similar for GL13K-TNTs and MNA-TNTs, but a slower release was achieved by GL13K-TNTs. This phenomenon might be because of the relatively strong interaction between GL13K and TNTs. As mentioned above, GL13K has a net charge of +5 at physiologic pH, while TNTs have a net negative charge under the same conditions.[34] Therefore, a strong electrostatic interaction was generated, leading to the reduced drug release rate.

The release profiles established in this study would enable implant sites to be sterilized in the initial stage. In addition, the subsequent continuous slow release would provide an effective prophylactic dosage to prevent infection for a longer duration. The presence of inhibition zones in the antimicrobial activity tests (Figure 5) indicates the effective antimicrobial activities of GL13K-TNTs and MNA-TNTs, even when they were exposed to high concentrations of bacteria. This study focused on the use of TNTs as local drug carriers for dental implants, and the cytocompatibility of this biocoating was also investigated in addition to its antimicrobial activity. GL13K-decorated coatings significantly promoted osteoblast attachment at the early stages. Furthermore, cell proliferation and ALP activity on TNTs with or without GL13K were similar, indicating that GL13K-TNTs could provide effective antimicrobial activity while not interfering with osteointegration.

Once implanted, an inflammatory response is immediately elicited at the site of surgery.[35] Macrophages are one of the cell types that arrive at the tissue–implant interface at the earliest time.[36] They display different phenotypes and play diverse roles in inflammation and wound healing depending on the location and stimulation conditions. Macrophages have been classified as classically activated (M1; proinflammatory) and alternatively activated (M2; immunomodulatory, tissue remodeling).[37] M1 cells mainly produce proinflammatory mediators such as interleukin-1β, interleukin-6, and tumor necrosis factor-α. In contrast, M2 cells are believed to play a predominant role in immunomodulation and tissue remodeling through different mechanisms.[38] It has been reported that M1 cells are predominant immediately following the initial inflammatory response, and then M1 cells undergo transition to an M2 phenotype with resolution of the inflammation.[39] It has been suggested that the favorable adherence and prolonged presence of macrophages could lead to healthy functional bone healing.[40] In this study, it was found that GL13K-TNTs did not interfere with the attachment and proliferation of J774A.1 murine macrophage cells, but, in fact, enhanced these properties. Cells spread out on the surfaces of TNTs and GL13K-TNTs, with numerous cytoplasmic lamellipodia on the rim and protrusions on the cell surface. Given that cell morphology regulates their function in part, perhaps the enhanced cell morphology on GL13K-TNTs would lead to positive outcomes in terms of tissue remodeling and bone healing. This is in accordance with other studies, which have shown that a charged hydrophilic surface contributes to better adsorption of adhesion proteins, thus inducing favorable cellular responses.[41] However, further work is still required to determine the role of adherent macrophage phenotypes and these molecules in bone healing sequences.

Importantly, it was also found that GL13K-TNTs are more cytocompatible with preosteoblast cells and macrophages than MNA-TNTs, which has been rarely reported previously. MNA-TNTs were chosen as the positive control for this study since MNA is considered to have a selective efficacy against anaerobes, which was confirmed and has been demonstrated in Figure 5. Despite a large number of supportive studies, there are insufficient data to outline the relevance of MNA to innate immunity or inflammation at implant sites. MNA functions by inhibiting DNA synthesis, and this mechanism is not only responsible for its antibacterial abilities, but is also associated with oxidative stress. Recently, a study has found that mitochondria can participate in innate immune pathways besides cellular metabolism or programmed cell death.[42] In this study, an MNA-mediated reduction in adhesion, proliferation, and changes in cell morphology in osteoblasts and macrophages, compared with the effects of TNTs and GL13K-TNTs, supports previous findings that MNA is immunosuppressive in terms of macrophage function in humans or experimental animal models.[43,44] However, these phenomena warrant further investigation.

Conclusion

Herein, it has been reported that TNTs processed using anodization could be used as a carrier for GL13K, the human parotid secretory protein-derived peptide, on implant surfaces. The antibacterial properties and biocompatibility of GL13K-TNTs indicate that they are suited as a local carrier of GL13K for early-stage prevention of infections at the implant sites and later promote osseous integration.

Acknowledgments

Disclosure

The authors report no conflicts of interest in this work.

References

1. Derks J, Tomasi C. Peri-implant health and disease. A systematic review of current epidemiology. *J Clin Periodontol*. 2015;42 (Suppl 16): S158–S171.
2. Darouiche RO. Device-associated infections: a macroproblem that starts with microadherence. *Clin Infect Dis*. 2001;33(9):1567–1572.
3. Eick S, Pfister W, Straube E. Antimicrobial susceptibility of anaerobic and capnophilic bacteria isolated from odontogenic abscesses and rapidly progressive periodontitis. *Int J Antimicrob Agents*. 1999;12(1):41–46.
4. Leonhardt Å, Renvert S, Dahlén G. Microbial findings at failing implants. *Clin Oral Implants Res*. 1999;10(5):339–345.
5. Jenkinson HF, Lamont RJ. Oral microbial communities in sickness and in health. *Trends Microbiol*. 2005;13(13):589–595.
6. Gristina AG, Naylor P, Myrvik Q. Infections from biomaterials and implants: a race for the surface. *Med Prog Technol*. 1989;14(14):205–224.
7. Duran LW. Preventing medical device related infections. *Med Device Technol*. 2000;11(6):14–17.
8. Norden CW. Antibiotic prophylaxis in orthopedic surgery. *Clin Infect Dis*. 1991;13 (Suppl 10):S842–S846.
9. Mombelli A, Samaranayake LP. Topical and systemic antibiotics in the management of periodontal diseases. *Int Dent J*. 2004;54(1):3–14.
10. Vasilev K, Cook J, Griesser HJ. Antibacterial surfaces for biomedical devices. *Expert Rev Med Devices*. 2009;6(5):553–567.
11. Rathbone CR, Cross JD, Brown KV, Murray CK, Wenke JC. Effect of various concentrations of antibiotics on osteogenic cell viability and activity. *J Orthop Res*. 2011;29(7):1070–1074.
12. Kazemzadeh-Narbat M, Kindrachuk J, Duan K, Jenssen H, Hancock RE, Wang R. Antimicrobial peptides on calcium phosphate-coated titanium for the prevention of implant-associated infections. *Biomaterials*. 2010; 31(36):9519–9526.
13. Hancock RE. Cationic peptides: effectors in innate immunity and novel antimicrobials. *Lancet Infect Dis*. 2001;1(3):156–164.
14. Gorr SU, Sotsky JB, Shelar AP, Demuth DR. Design of bacteria-agglutinating peptides derived from parotid secretory protein, a member of the bactericidal/permeability increasing-like protein family. *Peptides*. 2008;29(12):2118–2127.
15. Gorr SU, Abdolhosseini M, Shelar A, Sotsky J. Dual host-defence functions of SPLUNC2/PSP and synthetic peptides derived from the protein. *Biochem Soc Trans*. 2011;39(4):1028–1032.
16. Holmberg KV, Abdolhosseini M, Li Y, Chen X, Gorr SU, Aparicio C. Bio-inspired stable antimicrobial peptide coatings for dental applications. *Acta Biomater*. 2013;9(9):8224–8231.
17. Jenssen H, Hancock RE. Therapeutic potential of HDPs as immuno-modulatory agents. *Methods Mol Biol*. 2010;618:329–347.
18. Balamurugan A, Balossier G, Laurentmaquin D, et al. An in vitro biological and anti-bacterial study on a sol-gel derived silver-incorporated bioglass system. *Dent Mater*. 2008;24(10):1343–1351.
19. Chua PH, Neoh KG, Kang ET, Wang W. Surface functionalization of titanium with hyaluronic acid/chitosan polyelectrolyte multilayers and RGD for promoting osteoblast functions and inhibiting bacterial adhesion. *Biomaterials*. 2008;29(10):1412–1421.
20. Ma QL, Zhao LZ, Liu RR, et al. Improved implant osseointegration of a nanostructured titanium surface via mediation of macrophage polarization. *Biomaterials*. 2014;35(37):9853–9867.
21. Oh S, Jin S. Stem cell fate dictated solely by altered nanotube dimension. *Proc Natl Acad Sci*. 2009;106(7):2130–2135.
22. Popat KC, Eltgroth M, Latempa TJ, Grimes CA, Desai TA. Decreased Staphylococcus epidermis adhesion and increased osteoblast functionality on antibiotic-loaded titania nanotubes. *Biomaterials*. 2007; 28(32):4880–4888.
23. Wang N, Li H, Lü W, et al. Effects of TiO$_2$ nanotubes with different diameters on gene expression and osseointegration of implants in minipigs. *Biomaterials*. 2011;32(29):6900–6911.
24. Ma Y, Zhang Z, Liu Y, et al. Nanotubes functionalized with BMP2 knuckle peptide improve the osseointegration of titanium implants in rabbits. *J Biomed Nanotechnol*. 2015;11(2):236–244.
25. Liu W, Su P, Chen S, et al. Synthesis of TiO$_2$ nanotubes with ZnO nanoparticles to achieve antibacterial properties and stem cell compatibility. *Nanoscale*. 2014;6(15):9050–9062.
26. Lü W, Wang N, Gao P, Li CY, Zhao HS, Zhang ZT. Effects of anodic titanium dioxide nanotubes of different diameters on macrophage secretion and expression of cytokines and chemokines. *Cell Prolif*. 2015;48(1):95–104.
27. Uchida M, Kim HM, Kokubo T, Fujibayashi S, Nakamura T. Structural dependence of apatite formation on titania gels in a simulated body fluid. *J Biomed Mater Res A*. 2003;64(1):164–170.
28. Hirakawa Y, Jimbo R, Shibata Y, Watanabe I, Wennerberg A, Sawase T. Accelerated bone formation on photo-induced hydrophilic titanium implants: an experimental study in the dog mandible. *Clin Oral Implants Res*. 2013;24 (Suppl A100):139–144.
29. Balhara V, Schmidt R, Gorr SU, Dewolf C. Membrane selectivity and biophysical studies of the antimicrobial peptide GL13K. *Biochim Biophys Acta*. 2013;1828(9):2193–2203.
30. Hirt H, Gorr SU. Antimicrobial peptide GL13K is effective in reducing biofilms of Pseudomonas aeruginosa. *Antimicrob Agents Chemother*. 2013;57(10):4903–4910.
31. Chen R, Willcox MD, Cole N, et al. Characterization of chemoselective surface attachment of the cationic peptide melimine and its effects on antimicrobial activity. *Acta Biomater*. 2012;8(12):4371–4379.
32. Ma M, Kazemzadeh-Narbat M, Hui Y, et al. Local delivery of antimicrobial peptides using self-organized TiO2 nanotube arrays for peri-implant infections. *J Biomed Mater Res A*. 2012;100(2):278–285.
33. Lai S, Zhang W, Liu F, et al. TiO$_2$ nanotubes as animal drug delivery system and in vitro controlled release. *J Nanosci Nanotechnol*. 2013; 13(1):91–97.
34. Wang N, Lin H, Li J, Yang X, Chi B. Electrophoretic deposition and optical property of titania nanotubes films. *Thin Solid Films*. 2006; 496(2):649–652.
35. Anderson JM, Rodriguez A, Chang DT. Foreign body reaction to biomaterials. *Semin Immunol*. 2008;20(2):86–100.
36. Jones JA, Chang DT, Meyerson CH, et al. Proteomic analysis and quantification of cytokines and chemokines from biomaterial surface-adherent macrophages and foreign body giant cells. *J Biomed Mater Res A*. 2007;83(3):585–596.

37. Bowdish DM, Loffredo MS, Mukhopadhyay S, Mantovani A, Gordon S. Macrophage receptors implicated in the "adaptive" form of innate immunity. *Microbes Infect*. 2007;9(15):1680–1687.

38. Franz S, Rammelt S, Scharnweber D, Simon JC. Immune responses to implants–a review of the implications for the design of immunomodulatory biomaterials. *Biomaterials*. 2011;32(28):6692–6709.

39. Deonarine K, Panelli MC, Stashower ME, et al. Gene expression profiling of cutaneous wound healing. *J Transl Med*. 2007;5(1):1–11.

40. Brown BN, Londono R, Tottey S, et al. Macrophage phenotype as a predictor of constructive remodeling following the implantation of biologically derived surgical mesh materials. *Acta Biomater*. 2012;8(3): 978–987.

41. Wilson CJ, Clegg RE, Leavesley DI, Pearcy MJ. Mediation of biomaterial-cell interactions by adsorbed proteins: a review. *Tissue Eng*. 2005;11(2):1–18.

42. West AP, Shadel GS, Ghosh S. Mitochondria in innate immune responses. *Nat Rev Immunol*. 2011;11(6):389–402.

43. Fararjeh M, Mohammad MK, Bustanji Y, Alkhatib H, Abdalla S. Evaluation of immunosuppression induced by metronidazole in Balb/c mice and human peripheral blood lymphocytes. *Int Immunopharmacol*. 2008;8(2):341–350.

44. Han J, Zhang L, Yang S, Wang J, Tan D. Detrimental effects of metronidazole on selected innate immunological indicators in common carp (Cyprinus carpio L.). *Bull Environ Contam Toxicol*. 2014;92(2): 196–201.